Open Access Full Text Article

ORIGINAL RESEARCH

Biofabrication of Silver Nanoparticles Using *Nostoc muscorum* Lukesova 2/91: Optimization, Characterization, and Biological Applications

Reham Samir Hamida [1], Mohamed Abdelaal Ali[2], Fatima Tariq Sharif [3], Hana Sonbol [3], Mashael Mohammed Bin-Meferij[3]

[1]Institute for Protein Research, Osaka University, Osaka, 565-0871, Japan; [2]Plant Production Department, Arid Lands Cultivation Research Institute, City of Scientific Research and Technological Applications (SRTA-CITY) New Borg El-Arab, Alexandria, 21934, Egypt; [3]Department of Biology, College of Science, Princess Nourah bint Abdulrahman University, Riyadh, 11671, Saudi Arabia

Correspondence: Hana Sonbol, Department of Biology, College of Science, Princess Nourah bint Abdulrahman University, P.O.Box 84428, Email Hssonbol@pnu.edu.sa

Purpose: The biological synthesis of nanoparticles (NPs) has become a new methodology for the eco-friendly production of NPs with high scalability and biocompatibility. Cyanobacteria are one of the most widespread microorganisms on Earth and have been proven to be successful biofactories for synthesizing NPs. It is challenging to discover new microalgae with the potential to synthesize NPs of small size with high stability.

Methods: *Nostoc muscorum* Lukesova 2/91 was isolated, purified, and identified morphologically and genetically using microscopy and DNA sequencing. Volatile biomolecules in aqueous algal extracts were assessed using gas chromatography-mass spectroscopy (GC-MS).

Results: Data showed that the main biomolecules were fatty acids and their esters, followed by secondary metabolites. Algal extract was used to convert silver nitrate ($AgNO_3$) into silver NPs under various optimized parameters. 1 mM of $AgNO_3$, 1:1 (V/V ratio of algal extract to $AgNO_3$), 25 °C, under light illumination, for 24 h, at pH 7.4 were the optimum conditions for NP production (Nos@AgNPs). Nos@AgNPs were characterized using UV-VIS spectroscopy, FTIR, TEM, SEM, EDx, mapping, and a Zetasizer. The wavelength of Nos@AgNPs was 401.4 nm and their shapes were cubic to oval, with an average diameter of 11.8 ± 0.5 nm. FTIR spectroscopy revealed that proteins/polysaccharides could be the main reductants, whereas these molecules and/or fatty acids could be stabilizers for NP synthesis. Nos@AgNPs (86.15%) was silver and had a hydrodynamic diameter of 10.7 nm with a potential charge of −19.7 mV. Antiproliferative and antimicrobial activities of Nos@AgNPs were evaluated. Nos@AgNPs exhibited significant inhibitory activity against lung, colon, and breast cancer cells and considerable biocidal activity against *Staphylococcus aureus*, *Escherichia coli*, *Klebsiella pneumonia*, and *Pseudomonas aeruginosa*.

Conclusion: *N. muscorum* Lukesova 2/91 is an excellent source for the biofabrication of small and stable AgNPs with potent inhibitory effects against cancer and bacterial cells.

Keywords: green synthesis, algae, *Nostoc sp.*, antioxidant, anticancer, antimicrobial

Introduction

Physical and chemical methods are the most commonly used routes for fabricating NPs however their limitations such as high production costs, low scalability, energy consumption, and high-yield toxic substances limit their use.[1,2] To overcome these tackles, researchers have begun to use green synthesis to produce metals in nanoform. Green synthesis of nanoparticles (NPs) is one of the most reliable and sustainable techniques for NP production.[3] In the biological synthesis approach, precursors (metals) are reduced to their nanoforms using plants, lichens, cyanobacteria, fungi, and bacteria, or their purified biomolecules such as proteins, pigments, and polysaccharides.[4] This process has tremendous advantages, including eco-friendliness, high scalability, biocompatibility of NPs, and low consumption of money and energy.[5] By using green synthesis routes, researchers have been able to produce various metallic[6] and metallic oxide NPs[7] (MNPs and MONPs), as well as nanocomposites (NCs).[8] Cubic,[9]

spherical,[10] triangular,[9] and hexagonal[11] NPs have been synthesized using microalgae and cyanobacteria, whereas ZnO@SiO$_2$ NCs can be produced using lichen extract.[8]

Among MNPs, AgNPs have received great attention in the nanotechnology field because of their unique physicochemical characteristics, including small size, large surface-area-to-volume ratio, accessibility to modify their surfaces to obtain custom-tailored characteristics, and high reactivity of silver ions. They have great potential against various microbial and malignant cells.[12–14] AgNPs, synthesized using *Dunaliella salina*, with a small size of 35 nm, have shown significant biocidal activity against *Escherichia coli, Bacillus subtilis*, and *Enterobacter tobbaci*.[15] AgNPs synthesized by *Lyngbya majuscula* have shown significant antiproliferative activity against leukemia cells.[16] These exceptional properties enable the use of AgNPs in a wide range of applications such as biosensing,[17] drug delivery,[18] and biomedical devices for the diagnosis and detection of many diseases.[19,20]

Cyanobacteria are considered an enormous biofactory for synthesizing NPs because their cells contain numerous biomolecules such as proteins, polysaccharides, pigments, and enzymes, which act as reductants, and fatty acids, hydrocarbons, and oil, which act as stabilizers for NPs.[21] Researchers have successfully synthesized many MNPs and MONPs, including Ag,[9] Au,[22] Ti,[23] FeO,[24] and CuO.[25] They can also synthesize different shapes and sizes of the same metal.[9] *Nostoc* spp. are the most common soil cyanobacteria. They have nitrogen-fixing potential, which enables them to survive under wide temperature changes.[26] Additionally, they are rich in potent phytochemicals, such as phenolics, phycocyanin, triterpenoids, amino acids, polyunsaturated fatty acids, sulfate polysaccharides, and carotenoids. These bioactive compounds exhibit potent antimicrobial and antitumor activities.[27,28] *Nostoc muscorum* Lukesova 2/91 was isolated for the first time by Hrouzek et al from arable land in Nezamyslice/Czech Republic in 2005.[26]

The authors reported the main morphological features of these species, including long coiled filaments, diffusive mucilaginous sheaths, terminal oval heterocytes that exist mainly after disruption of the filament, and oval akinetes that germinate into long vegetative filaments. In another report published by Hrouzek and colleagues, the authors studied the cytotoxicity of methanolic fractions of various *Nostoc* species and one was *Nostoc muscorum* Lukesova 2/91.[29] The data showed that *N. muscorum* Lukesova 2/91 extract exhibited moderate toxicity against both YAC-1 (murine lymphoblasts, induced by Moloney leukemia virus) and Sp/2 (murine myeloma cells). However, only one fraction of this extract caused 45% inhibition of Sp/2, similar to the crude extract (53%). Despite the fact that cyanobacteria are a promising biomachinery for NP synthesis, the potential of new species and strains to biofabricate small and stable NPs is still unknown. Furthermore, controlling the size and shape of NPs remains a significant issue in biofabrication methods. Researchers recently reported computational and traditional optimization processes for NPs synthesis. They discovered that the synthetic factors such as pH, temperature, concentrations, time of exposure, etc. influence the size and shape of NPs.[30,31]

Herein, we synthesized AgNPs using a novel strain of *Desmonostoc* species for the first time and report their phytochemical content and potential for biofabricating AgNO$_3$ into small AgNPs. We optimized the synthesis of AgNPs to yield smaller and more stable NPs by altering various abiotic factors. The Nos@AgNPs were physicochemical characterized and assessed against various malignant and microbial cells.

Materials and Methods
Materials

All chemicals and kits, including chemically synthesized AgNPs (Ch@AgNPs, 576832, with a size of 100 nm and spherical shape, 99.5% purity) and MTT kit (M2128), were purchased from Sigma-Aldrich (St. Louis, MO, USA). Gibco (Thermo Fisher Scientific, Waltham, MA, USA) provided media and tools for cell culture, while the dye resazurin was obtained from BDH Chemicals, England. Lung cell line A549, breast cancer T47D cells, MCF-7ADR, MDA-MB231, and normal human fibroblasts (HFs), and African green monkey kidney (Vero) cells were procured from Nawah Scientific Company, Cairo, Egypt (which obtained them from ATCC, Manassas, VA, USA). Microbial isolates used in this study were obtained from the Department of Microbiology at King Saud University, Riyadh, Saudi Arabia.

Methods

Isolation, Purification, and Microalgae Cell Culture

Soil samples (10 g of upper soil layer) from Riyadh, Saudi Arabia, were collected in sterile 50 mL Falcon tubes and brought to the laboratory. Samples were then incubated for one week on a sterile Petri dish with 20 mL BG11 medium (BG11 media was prepared according to Havel et al recipe[32]) in an incubator under a fluorescence lamp (2000 ± 200 Lux) with 12:12 h dark and light cycles. To purify the samples, various steps including serial dilution and BG11 agar plating were performed as described by Bolch et al and Hamida et al.[11,33] Aliquots of the purified samples were cultured under the above-mentioned conditions for 15 days in 1000 mL flasks containing BG11 medium for large-scale cyanobacterial growth.

Morphological Identification of Microalgae

To verify the purity and morphological characteristics of the cyanobacterial samples, purified colonies were incubated in sterile test tubes and examined under light (Novex, Holland, The Netherlands) and inverted (Thermo Fisher Scientific, USA) light microscopes.

16s rRNA Sequencing and Bioinformatic Analysis

DNA was extracted from cyanobacteria using a DNA extraction kit (Attogene, Austin, TX, USA) according to the manufacturer's instructions. PCR (PeqSTAR 96X universal gradient thermal cycler, VWR, UK) was used to amplify the DNA according to Weisburg et al[34] in which cycling parameters were 94 °C for 1 min followed by 35 cycles of 95 °C for 30s, 55°C for 1 min, 74 °C for 2 min and a final extension of 72 °C for 5 min. A forward primer 5'-AGAGTTTGATCCTGGCTCAG-3' and reverse primer 5'-GGCTACCTTGTTACGACTT-3' were used for amplification. Amplicons were stored in nuclease-free water and sent to Macrogen (Seoul, Korea) for DNA sequencing.

Gas Chromatography–Mass Spectrometry (GC-MS) Analysis

Thermo Fisher Scientific's Trace GC-TSQ mass spectrometer and a direct capillary column TG-5MS (30 m 0.25 mm 0.25 m film thickness) were used to screen volatile components in the *N. muscorum* Lukesova 2/91 aqueous extract. Briefly, 50 mg algal powder was sonicated in 50 mL boiling distilled water H_2O for 30 min. The sample was then allowed to macerate for 24 h before being filtered through a 0.22 μm syringe filter. The filtrate was dried for 48 h at 50 °C in a vacuum oven. All GC-MC performance conditions are described in detail in our previous study.[11] The mass spectra of the algal extracts were compared with those in the WILEY 09 and NIST 14 mass spectral databases to determine their constituents.

Preparation of Algal Extracts

The cyanobacterial biomass was separated by centrifugation at 4700 rpm for 10 min, washed three times with deionized water, and lyophilized for 24 h using LYOTRAP (LTE Scientific, Greenfield, UK). Equal amounts of algal powder were dissolved in distilled water and then the mixture was boiled at 80 °C for 30 min to create an aqueous extract. The mixture was then centrifuged at 4700 rpm for 10 min, and the supernatant was filtered using Whatman filter paper No. 1 and immediately used for NP biofabrication.

Optimization Process of AgNP Synthesis Using *N. Muscorum* Lukesova 2/91

Numerous parameters were evaluated to determine the ideal conditions for Nos@AgNP biofabrication. These parameters included precursor concentration, algal/precursor (v/v) ratio, temperature, illumination conditions, pH, and incubation time. To determine the ideal concentrations and ratios, Nos@AgNPs were first produced using different concentrations (1, 2, 5, and 10 mM) of silver nitrate at a constant ratio of 1 to 1 (algal extract to silver nitrate) and a temperature of 25 °C under illumination for 24 h. UV-VIS spectroscopy (Shimadzu, Japan) was used to screen the synthesized Nos@AgNPs produced at each concentration. The effects of various algal extracts and precursor ratios were assessed following the determination of optimal concentrations. Under the same constant conditions, four ratios were evaluated by combining algal extract with 1 mM of $AgNO_3$ at ratios of 1:1, 1:2, 1:4, and 1:9 (algal extract to $AgNO_3$).

In order to assess how temperature affects NP biofabrication, 1 mL of 1 mM $AgNO_3$ was mixed with 1 mL of algal extract (at 1:1 ratio), and the mixture was subjected to different temperatures of 25, 40, 60, and 100 °C for 1 h under

other constant conditions. After reaching the optimum temperature (25 °C), the pH values of $AgNO_3$ and the algal extract mixture were changed using 0.1 M hydrochloric acid or sodium hydroxide to be 5, 7, 7.8 (original pH of the mixture without any changes), 9, and 12 under the same constant conditions for NP synthesis.

Furthermore, a 1:1 mixture of $AgNO_3$ and algal extract was thoroughly mixed at 25 °C and a pH of 7.8 before being incubated for 24 h, once in the dark and once in the light (using a fluorescent lamp with 2000 ± 200 Lux). This was performed to obtain the optimum illumination conditions. The mixture was also tested by incubating it under light for 24 and 48 h to determine the impact of incubation time on NP biofabrication. After determining the ideal conditions for the biogenesis of Nos@AgNPs, NPs were produced in large quantities (3 L), centrifuged at 15,000 rpm for 15 min, washed at least three times with deionized water, and lyophilized for 8 h. To prepare for subsequent research, the powdered NPs were weighed and placed in sterile Eppendorf tubes.

Physicochemical Characterization of Optimum AgNPs

UV-Spectroscopy
An aliquot (2 mL) of Nos@AgNPs was examined using UV spectroscopy at a resolution of 1 nm over a wavelength range of 200–800 nm for each optimal parameter.

Transmission and Scanning Electron Microscopy, EDx and Mapping
Transmission electron microscopy (TEM, JEM-1400Flash, Joel, Japan) and scanning electron microscopy (SEM, JSM-IT500HR, Joel, Japan) were used to examine the size and shape of Nos@AgNPs. In order to conduct a TEM examination at 120 kV, a suspension of Nos@AgNPs was sonicated for 15 min and 10 µL of the suspension was dropped onto a carbon-coated copper grid and allowed to dry at room temperature. Samples were prepared for SEM, EDx, and mapping examination as follows: dried Nos@AgNP powder was placed on clean clinic paper and transferred onto a carbon paste strip, which was affixed to a copper stub. The stubs were knocked with a smooth motion to eliminate additional powder. An auto-fine coater was used to apply a layer of platinum to the sample, which was then subjected to 15 kV SEM analysis. EDx detector (STD-PC80, Joel, Japan) and SEM operating software were used to determine the chemical composition and distribution of the coated samples.[35]

Zeta Potential and DLS
To measure the hydrodynamic diameter (HD) and potential charge of the Nos@AgNP suspensions, A Zetasizer (Malvern, UK) was used. The Nos@AgNP suspensions were diluted tenfold with distilled H_2O, sonicated for 15 min, and then transferred into U-type tubes before measurement with the Zetasizer at 25 °C.

FTIR
FTIR spectroscopy (Shimadzu, Kyoto, Japan) was used to analyze the functional groups used to coat the surface of Nos@AgNPs over a spectral range of 400 to 4000 cm^{-1}.

Anticancer Activity of AgNPs
Six cancer cell lines, including T47D, MDA-MB231, MCF7, MCF7-ADR, SW480, and A549, as well as two normal cell lines: Vero and HFs were cultured in an incubator at 37 °C with 5% carbon dioxide, in full DMEM and RPMI medium containing 10% fetal bovine serum and 50 U/mL penicillin and streptomycin. The cells were passaged using trypsin-EDTA, counted, seeded into 96-well plates at a density of 5×10^4 cells/well, and incubated for 24 h under the same conditions.

The cytotoxicity of Nos@AgNPs, Ch@AgNPs, doxorubicin (Doxo) and 5-fluorouracil (5-FU) against selected cells was determined using the MTT assay. Of note, Ch@AgNPs were assessed against only MCF-7ADR, Sw480 and A549, while 5-FU were screened against MCF-7ADR and A549 cells. Other cells were previously tested against both Ch@AgNPs and 5-FU in our previous publications.[11,35,36] To validate Nos@AgNP activity, Doxo, 5-FU, and Ch@AgNPs were used as positive controls. First, 1 mg of Nos@AgNPs, Ch@AgNPs, Doxo, and 5-FU was dissolved in 1 mL DMEM. Nos@AgNPs and Ch@AgNPs were sonicated for 15 min to ensure that all particles were suspended in the medium, whereas Dox and 5-FU were vortexed for 1 min. The NP, Doxo, and 5-FU solutions were then filtered using a 0.45 µm pore size microfilter. The grown cells were subsequently subjected to various concentrations of filtered

Nos@AgNPs (500, 250, 125, 62.5, 31.25, 15.62, 7.81, 3.90, and 1.95 µg/mL), Ch@AgNPs, Doxo, and 5-FU (1000, 500, 250, 125, 62.5, 31.25, 15.62, 7.81, and 3.90 µg/mL) and incubated at 37 °C for 24 h. After this, the medium was removed, and 100 µL/well of fresh medium was added. Next, 10 µL of MTT solution (5 mg/mL) was added to each well, and the solution was combined with the medium. The treated plates were incubated in the dark at 37 °C for 4 h. After incubation, 100 µL of DMSO was added to each well in order to dissolve the formazan crystals, and the plates were then subjected to rotary agitation for 15 min at 400 rpm. The optical absorbance was measured at 570 nm.[4] The following equation was used to determine the percentage of viable cells: (Abs(treated)/(Abs(control)) × 100.

Antimicrobial Activity of AgNPs

Escherichia coli, Klebsiella pneumoniae, and Pseudomonas aeruginosa are all gram-negative bacteria, whereas *Staphylococcus aureus* is a gram-positive bacterium. These four bacterial strains were cultured in nutrient broth for up to 18 h at 37 °C, and maintained by continuously subculturing them in broth and on agar media.

Agar-Well Diffusion Method

The agar-well diffusion approach was used to assess the antimicrobial activity of 1 mg/mL of Nos@AgNPs, AgNO$_3$, Ch@AgNPs, algal extract, and 5 µg/mL ciprofloxacin against all tested bacteria as follows: 4 mL of bacterial suspension (2.5–3.6 × 10^6 CFU/mL) was suspended in 50 mL of nutrient agar media. The mixture was poured into sterile Petri dishes and dried at 37 °C. Wells (8-mm diameter) were created on the agar plates using a cork borer. Subsequently, 100 µL of Nos@AgNPs, AgNO$_3$, Ch@AgNPs, ciprofloxacin, and algal extract suspensions were poured into the 8 mm wells. The plates were placed in a bacterial incubator at 37 °C for 24 h. Diameters of the inhibition zone (mm) were determined using a transparent ruler.[2]

Minimum Inhibitory and Bactericidal Concentrations

The minimum inhibitory and bactericidal concentrations (MIC and MBC, respectively) of Nos@AgNPs were determined using the resazurin dye method described by Elshikh et al.[3] Serial dilutions of Nos@AgNPs (500, 250, 125, 62.5, 31.25, 15.62, 7.8, 3.9, 1.95, and 0.98 µg/mL) were prepared and 100 µL of each concentration was mixed with 100 µL bacterial suspension (2.5–3.6 × 10^6 CFU/mL). A positive control consisting of an untreated bacterial suspension and a negative control (media only to monitor sterility) were used. After that, the plates were kept in an incubator overnight at 37 °C. After 24 h, 30 µL of resazurin dye solution (0.015%) was delivered into each well of the plate, and kept in an incubator set to 37 °C for a period of 4 h. Optical absorbance was measured at 570 nm using a plate reader (Bio-Rad, USA). After 4 h, the column was considered above the MIC value if there was no color change (the color of the resazurin indicator, blue, remained the same). MBC values were calculated by depositing the contents of wells with concentrations > MIC on nutrient agar plates. MBC values indicated the lowest concentration of the biocidal agent at which the plates did not exhibit any signs of colony growth.

Statistical Analysis

Data are presented as means ± standard error of the mean (SEM) of three independent replicates for each experiment. Differences between control and experimental groups were analyzed using one-way analysis of variance (ANOVA) in GraphPad Prism v.9.3.1 (GraphPad Software Inc., San Diego, CA, USA) and statistical significance was set at a *p* value of < 0.05. Origin 8 (OriginLab Corporation, Northampton, MA, USA) and ImageJ (National Institutes of Health, Bethesda, MD, USA) software was used to determine the physicochemical characteristics of Nos@AgNPs.

Results and Discussion
Morphological and Genetic Identification of Cyanobacteria

Light and inverted micrographs of the tested species demonstrated that the isolate had blue-green isodiametric to barrel-like trichomes (Figure 1). This morphological analysis suggested that the isolate belongs to the *Nostocaceae* family. Our results agree with those of Hrouzek et al, who reported that this isolate has coiled filaments, a diffusive mucilaginous sheath, terminal oval heterocytes that exist mainly after disruption of the filament, and oval akinetes that germinate into long vegetative filaments.[26] *16s* rRNA sequence analysis showed that the present isolate was 100% identical to
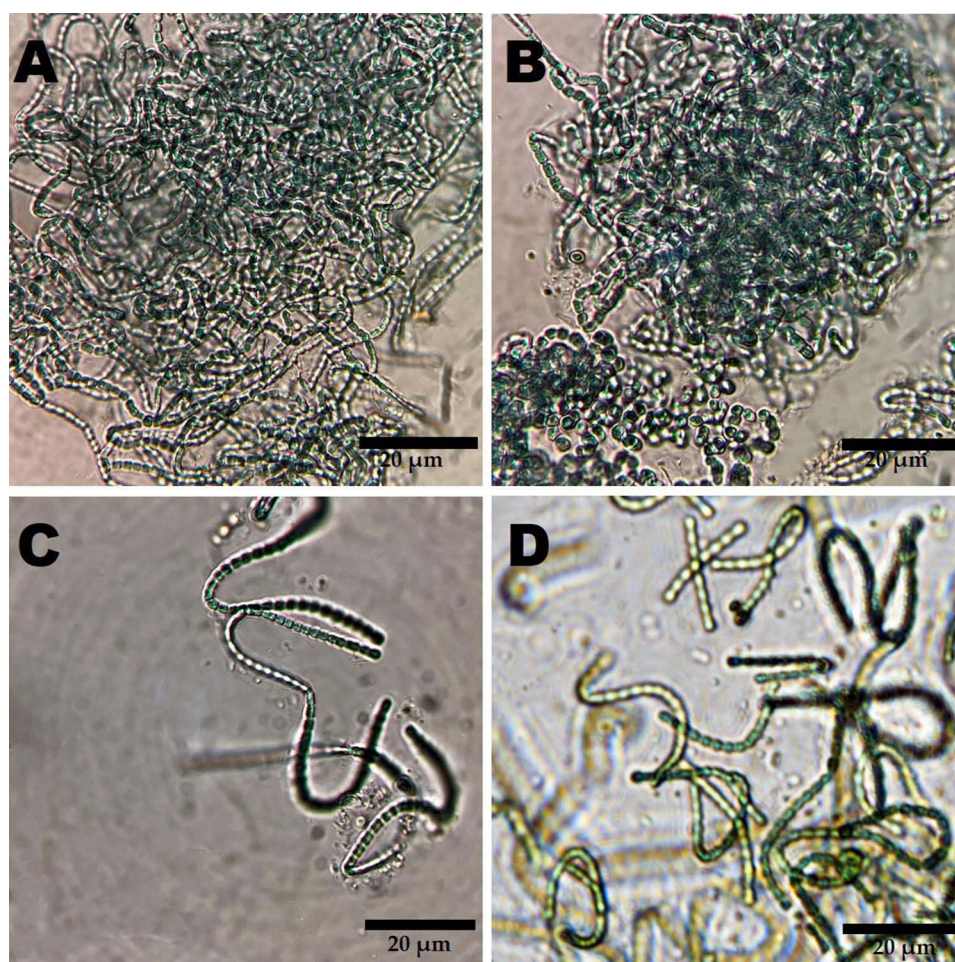
Figure 1 Light (**A-C**) and inverted light (**D**) micrographs illustrating the barrel-like filaments of *N. muscorum* Lukesova 2/91. Scale bar = 20 µm.

N. muscorum Lukesova 2/91. Isolate sequences were recorded in GenBank and the National Center for Biotechnology Information (NCBI) with accession numbers OQ878272. A phylogenetic tree revealed that the current species clustered within *Desmonostoc* sp (Figure 2).
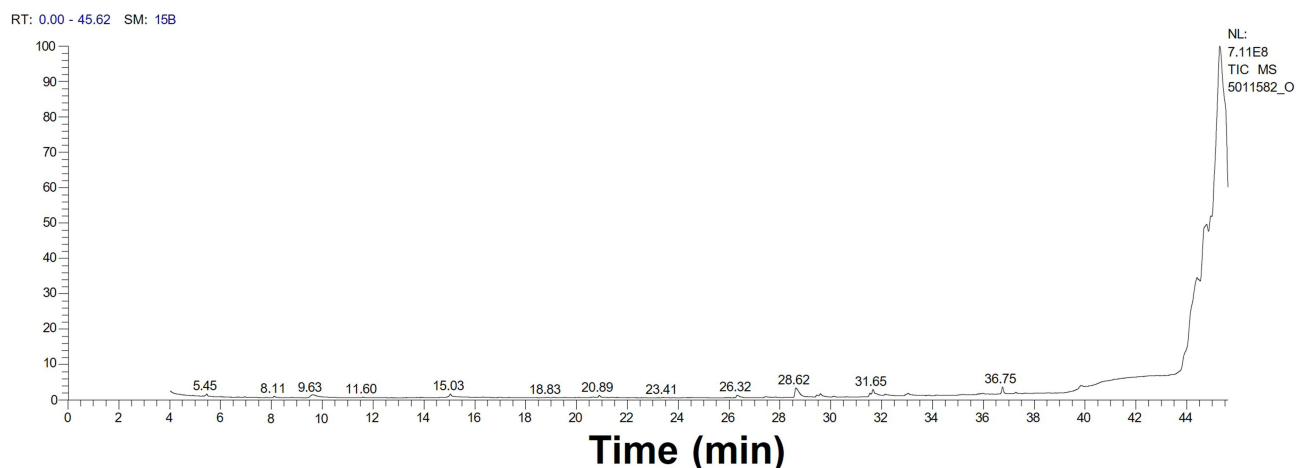
GC-MS Analysis

The GC-MS chromatogram of *Nostoc muscorum* Lukesova 2/91 aqueous extract exhibited 16 peaks corresponding to 16 volatile biomolecules over the retention time range of 4–44 min (Figure 3 and Table 1). Organic molecules included fatty acids, fatty acid esters, phenylpropenes, sesquiterpenoids, sesquiterpenoid tertiary alcohols, vitamin D derivatives, and carboxylic acids. The main compounds in the watery extract were fatty acids and their esters, suggesting that these organic compounds may precipitate during the synthesis of Nos@AgNPs as stabilizing agents. However, the presence of both sesquiterpene and sesquiterpenoid tertiary alcohols indicates that secondary metabolites may play a significant role in the reduction of $AgNO_3$ to AgNPs. It was found that the watery extract of *N. muscorum* Lukesova 2/91 had a variety of significant biomolecules, such as ethyl cholate, which is highly cytotoxic against lung cancer A549 cells with zero toxicity toward zebrafish[37] and estragole, which enhances the apoptotic pathway in MCF-7, causing DNA damage, chromatin condensation, and membrane disruption.[38] Patchouli alcohol has potent antibacterial efficacy against *E. coli*, *P. aeruginosa*, *B. proteus*, *Shigella dysenteriae*, *Typhoid bacillus*, and *S. aureus*.[39] Additionally, fatty acid esters such as 8.11-octadecadienoic acid methyl ester exhibit great antioxidant activity.[40] Caryophyllene-(I1) has significant antibacterial, re-epithelialization, and anti-inflammatory properties.[41] El-Fayoumy et al reported that *Nostoc linckia* contains
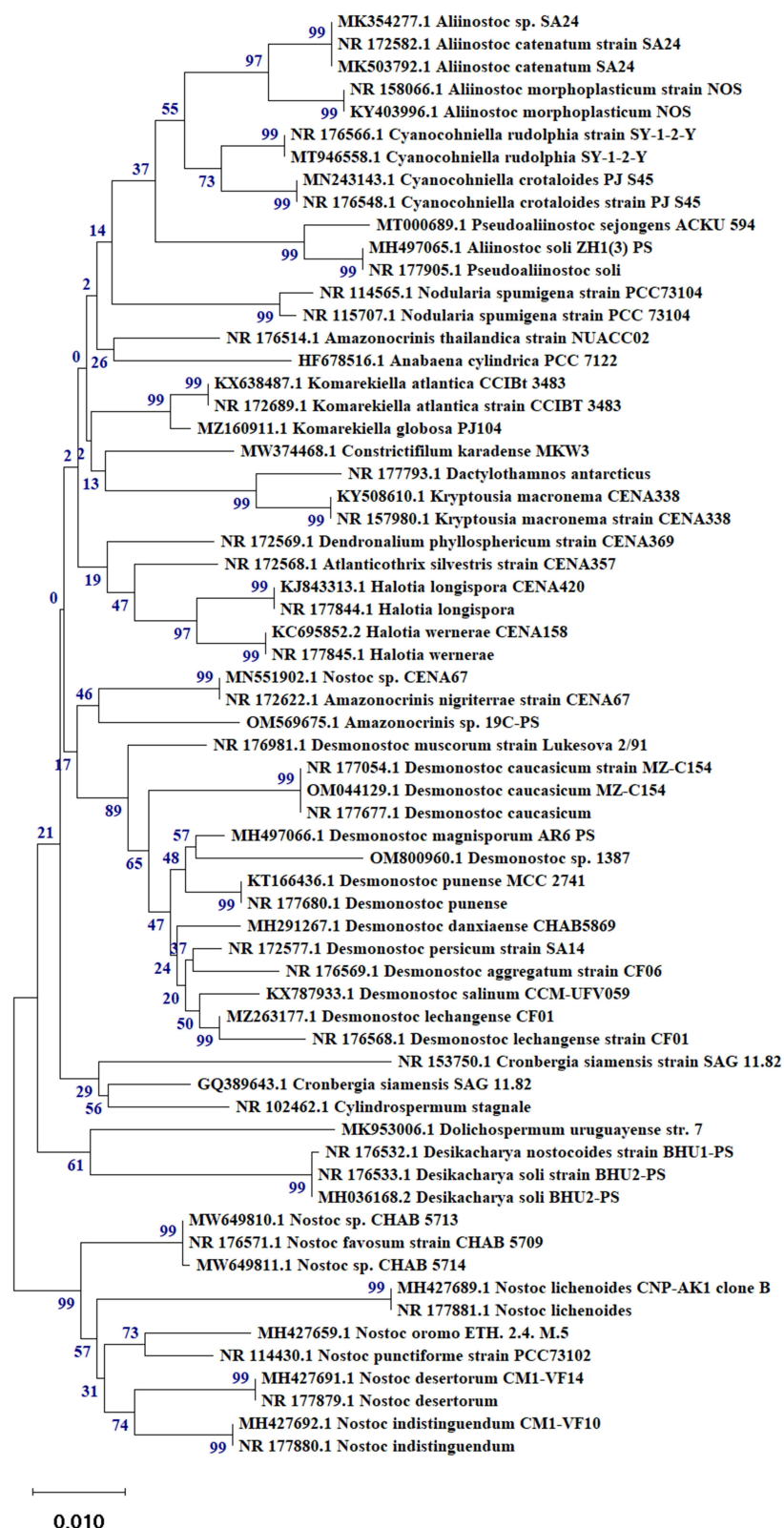
Figure 2 Phylogenetic tree of *N. muscorum* Lukesova 2/91 inferred from 16S rRNA and constructed by cluster method using MEGA4 software version 10.2.6. The number at each branch refers to the bootstrap values for % of 1000 replicate trees calculated by the neighbor-joining method.

Figure 3 GC-MS chromatogram of *N. muscorum* Lukesova 2/91 aqueous extract illustrating 16 peaks corresponding to 16 volatile biomolecules over a retention time range of 4–44 min.

various biomolecules that serve as antioxidant, antimicrobial, anticancer, and antiviral agents.[42] These molecules include cyclohexasiloxane, dodecamethyl, cycloheptasiloxane, tetradecamethyl, 2-hexadecen-1-ol, 3,7,11,15-tetramethyl-, 1.2-benzenedicarboxylic acid, diisooctyl ester, 2-hexadecanol, hexadecanoic acid, and methyl ester.
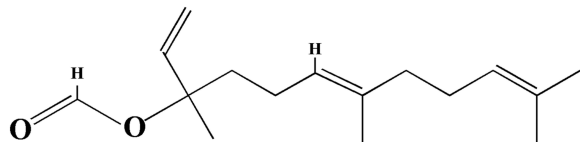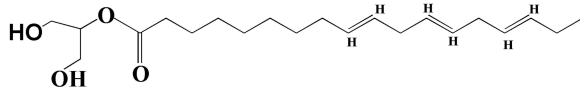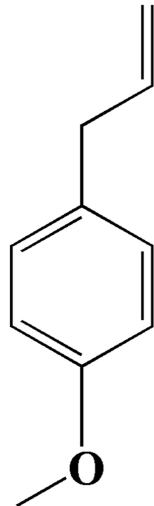
Optimization Parameters for Nos@AgNP Synthesis Using *N. Muscorum* Lukesova 2/91

UV spectral data demonstrated that the precursor concentration significantly influenced NP size. The wavelengths of Nos@AgNPs resulting from the reaction between the algal extract and 1, 2, 5, and 10 mM $AgNO_3$ were 401.4, 413, 423, and 432 nm. Figure 4A illustrates that the peak of Nos@AgNPs at 1 mM was narrower than those at 2, 5, and 10 mM, explaining a better degree of nanoparticle distribution. An increase in the concentration of $AgNO_3$ with other constant parameters resulted in an increase in the average crystallite size or agglomeration rate.[43] This could be attributed to the fact that increasing the initial concentration of Ag ions in the presence of a constant volume of reductant (algal extract) could result in an unbalanced reaction in which the number of reductants and stabilizers was insufficient to form stable NPs, encouraging the formation of agglomerates via intermolecular reactions.[44]

The data also revealed that algal/$AgNO_3$ (V/V) ratio influenced the size of Nos@AgNPs. The increase in the volume of silver ions against a constant volume of algal extract redshifted the wavelength of NPs. For instance, at 1:1, 1:2, 1:4, and 1:9 algal to $AgNO_3$ (V/V) ratios, Nos@AgNPs formed at wavelengths of 401.4, 402, 414, and 406 nm, respectively. Intriguingly, at 1:1 and 1:2 algal to $AgNO_3$ (V/V) ratios, Nos@AgNPs had narrower absorption peaks at approximately similar wavelengths, whereas at 1:4 algal to $AgNO_3$ (V/V) ratio, the absorption peak became broader than that at 1:1 and 1:2, suggesting the formation of large NPs (Figure 4B). At a 1:9 algal to $AgNO_3$ (V/V) ratio, Nos@AgNPs had the broadest peak and lowest intensity compared to those at other ratios, indicating that large NPs or more aggregates were formed.[45]

The influence of temperature change on the synthesis of Nos@AgNPs was investigated by mixing 1 mL of 1 mM of $AgNO_3$ with 1 mL of algal extract and kept at 25, 40, 60, and 100 °C (Figure 4C). It was found that wavelength values of Nos@AgNPs at 25, 40, 60, and 100 °C were 401.4, 402.4, 409.4, and 381.4 nm, respectively. These data clarified that both 25 and 40 °C were suitable for activating biomolecules responsible for synthesizing small NPs. However, upon increasing the temperature to 60 °C, a broader absorption peak appeared with higher wavelength values compared to those at 25 and 40 °C, suggesting that temperature increments enhanced the self-assembly of NPs or increased NP sizes.[46] This could be attributed to the exposure of the reaction mixture to high temperatures, which may deactivate the biomolecules responsible for reducing or stabilizing NPs by denaturing their structure. This conclusion was confirmed when the temperature was increased to 100 °C, as no Nos@AgNPs formed.
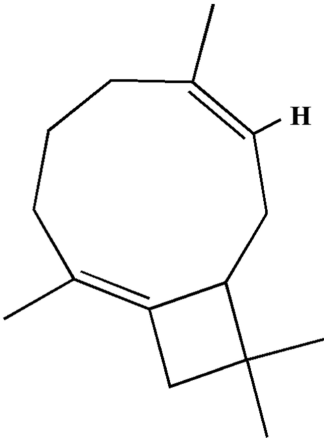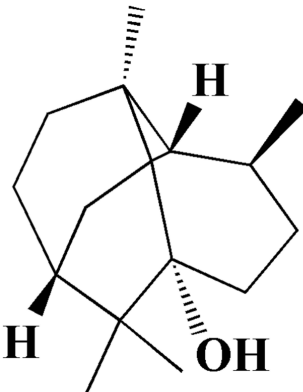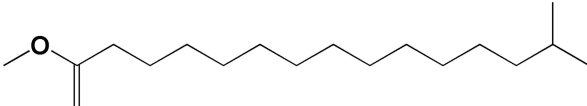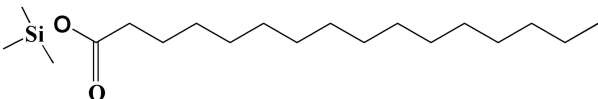
5633

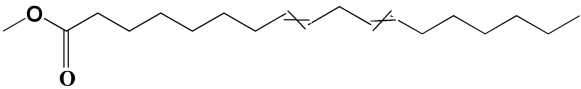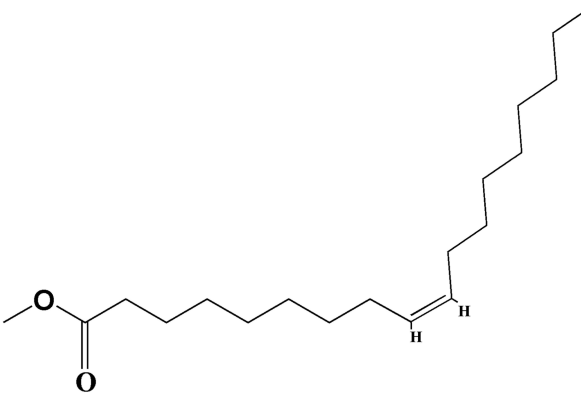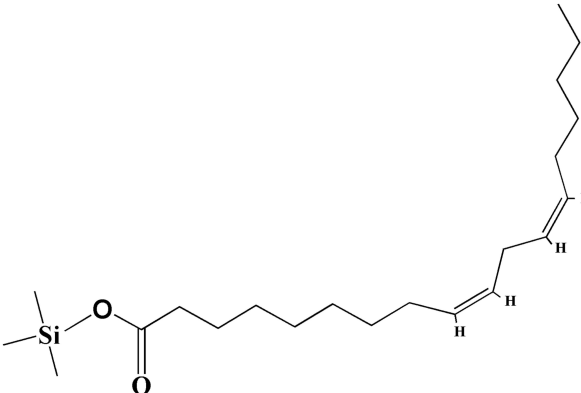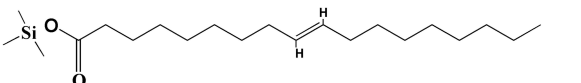**Table 1** GC-MS Spectra of Volatile Phytochemicals of *N. Muscorum* Lukesova 2/91 Aqueous Extract

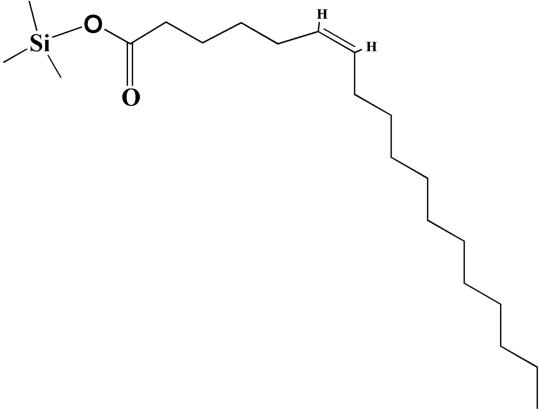| No.	RT	Compounds	Area %	Matched Factor	Molecular Formula	Molecular Weight	Chemical Structure
1	5.46	Formic acid, 3,7,11-trimethyl-1,6,10-dodecatrien-3-yl ester	3.40	724	$C_{16}H2_6O_2$	250	
2	8.11	Linolenic acid, 2-hydroxy-1-(hydroxymethyl)ethyl ester (Z,Z,Z)-	2.05	737	$C_{21}H_{36}O_4$	352	
3	9.61	Estragole	7.13	900	$C_{10}H_{12}O$	148	

(*Continued*)
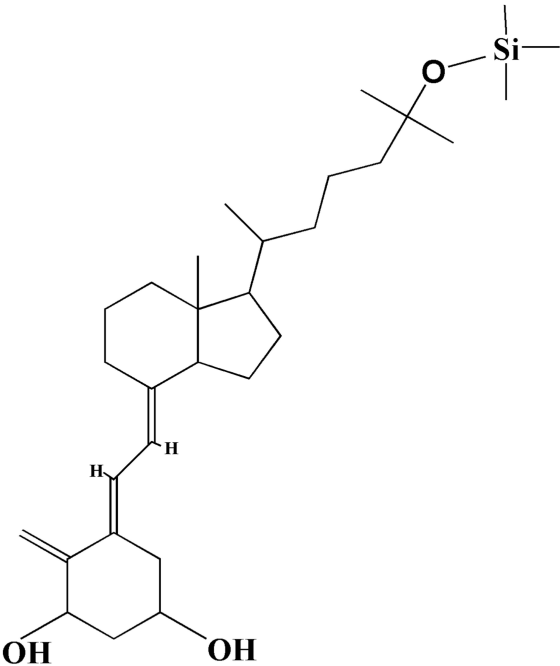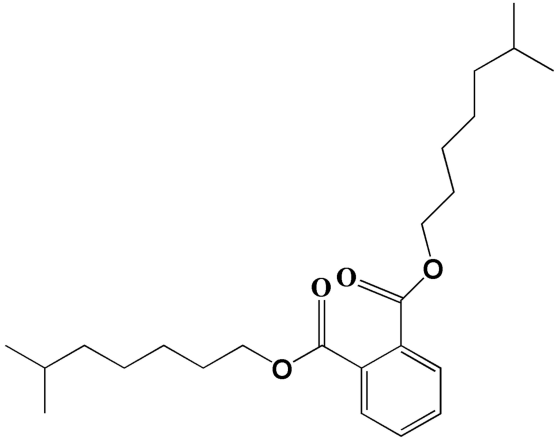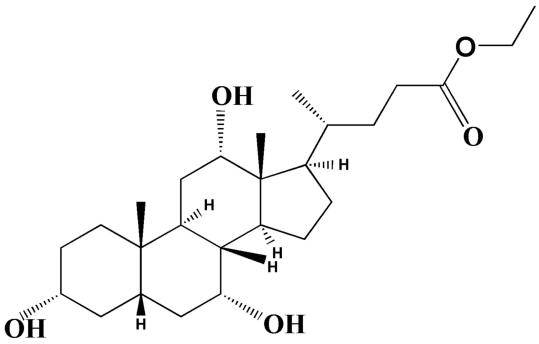
Hamida et al

Table 1 (Continued).

No.	RT	Compounds	Area %	Matched Factor	Molecular Formula	Molecular Weight	Chemical Structure
4	15.03	Caryophyllene-(I1)	4.79	902	$C_{15}H_{24}$	204	
5	20.89	Patchouli alcohol	**2.93**	**870**	$C_{15}H_{26}O$	**222**	
6	26.31	Methyl 14-methylpentadecanoate	4.31	745	$C_{17}H_{34}O_2$	270	
7	28.62	Hexadecanoic acid, trimethylsilyl ester	17.36	896	$C_{19}H_{40}O_2Si$	328	

8	29.45	8,11-Octadecadienoic acid methyl ester	3.37	810	$C_{19}H_{34}O_2$	294	
9	29.59	Methyl cis-9-octadecenoate	7.14	851	$C_{19}H_{36}O_2$	296	
10	31.54	Linoleic acid trimethylsilyl ester	5.24	873	$C_{21}H_{40}O_2Si$	352	
11	31.66	Trimethylsilyl (9E)-9-octadecenoate	17.05	835	$C_{21}H_{42}O_2Si$	354	

(*Continued*)
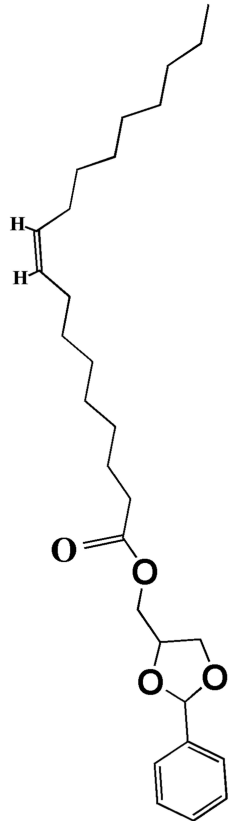
Table 1 (Continued).

No.	RT	Compounds	Area %	Matched Factor	Molecular Formula	Molecular Weight	Chemical Structure
12	32.14	(Z)-6-Octadecenoic acid trimethylsilyl ester	2.16	717	$C_{21}H_{42}O_2Si$	354	
13	33.03	(5E,7E)-25-[(Trimethylsilyl)oxy]-9,10-secocholesta-5,7,10-triene-1,3-diol #	3.17	774	$C_{30}H_{52}O_3Si$	488	

14	36.75	1,2 Benzene dicarboxylic acid, diisooctyl ester	10.74	925	$C_{24}H_{38}O_4$	390	
15	37.27	Ethyl cholate	2.19	774	$C_{26}H_{44}O_5$	436	

(*Continued*)

5638

International Journal of Nanomedicine 2023:18

Table 1 (Continued).

No.	RT	Compounds	Area %	Matched Factor	Molecular Formula	Molecular Weight	Chemical Structure
16	39.83	(2-Phenyl-1,3-dioxolan-4-yl)methyl 9-octadecenoate, cis-	6.96	800	$C_{28}H_{44}O_4$	444	
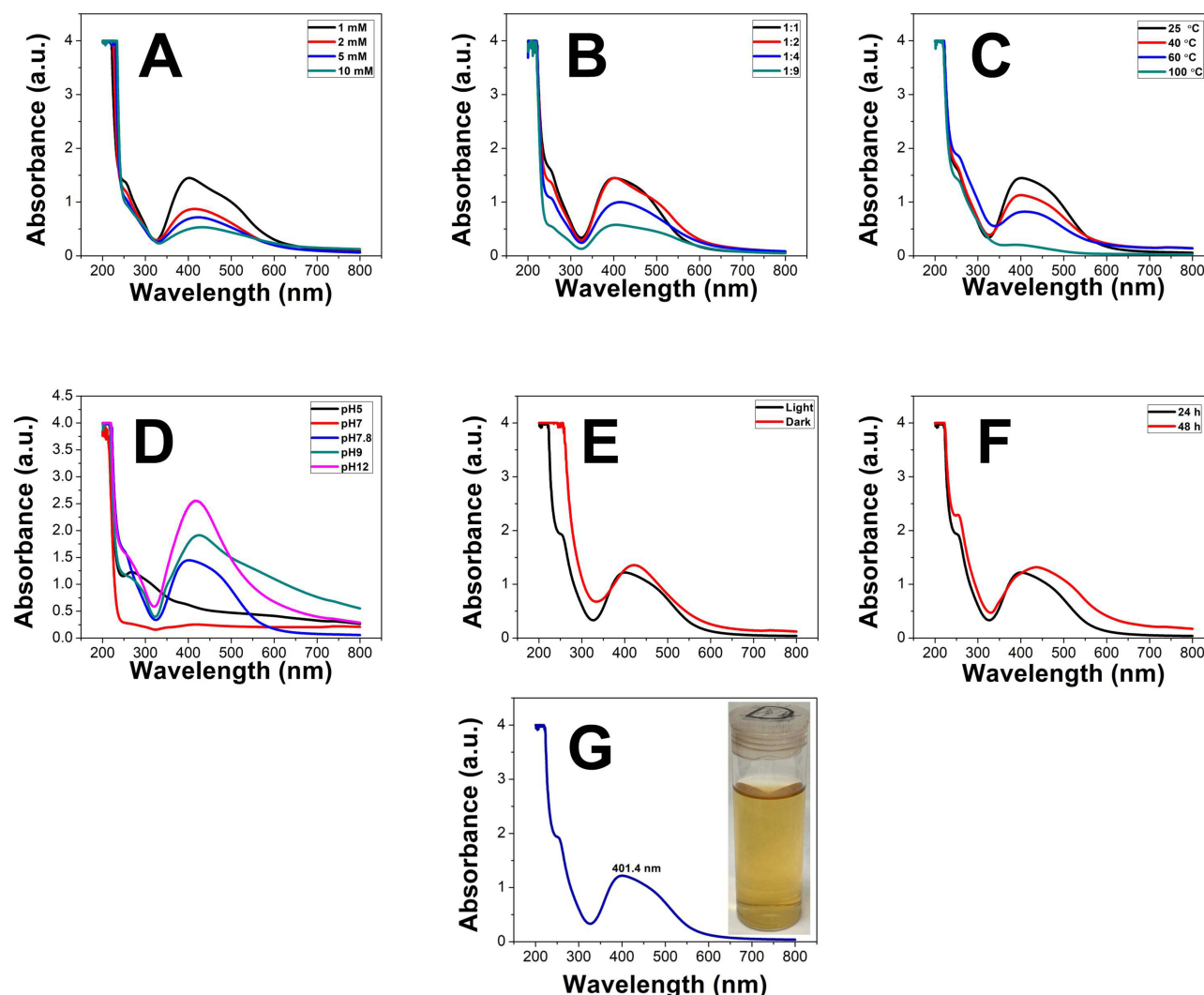
Figure 4 Wavelength (nm) of Nos@AgNPs synthesized by *Nostoc muscorum* Lukesova 2/91 at various optimization parameters of precursor concentration (**A**), algal to precursor ratio (V/V) (**B**), temperature (**C**), pH (**D**), illumination condition (**E**), incubation time (**F**), and final optimized Nos@AgNPs (**G**).

The data showed that adjusting the pH of the mixture of $AgNO_3$ and algal extract to pH 5, pH 7, original pH (7.8), pH 9, and pH 12 using Tris HCl or NaOH significantly affected NP size and stability (Figure 4D). At pH 5, AgNPs were not formed, while at pH 7, original pH (7.8), pH 9, and pH 12, Nos@AgNPs were formed with a wide range of wavelengths, including 420, 401.4, 425.2 and 416.5 nm. At pH 9 and 12, Nos@AgNPs had the highest intensity and a sharper absorption peak, suggesting the production of uniform NPs of larger sizes. Intriguingly, the optimum pH to synthesize small and stable Nos@AgNPs was original pH (7.8) at a wavelength of 401.4 nm. Changing the pH above or below the optimum value enhances the self-assembly of NPs or increases their size.[47]

To study the influence of light exposure on the synthesis of Nos@AgNPs, a mixture of $AgNO_3$ and algal extract under optimum conditions was maintained under dark and light conditions. The data showed that the absorption peaks of reactions exposed to light were at a wavelength of 401.4 nm, whereas those kept in the dark were at a wavelength of 423.5 nm. These data suggested that the synthesis of Nos@AgNPs using *N. muscorum* Lukesova 2/91 may depend on light energy to accelerate the reduction process. Additionally, increasing the exposure time to light from 24 h (401.4 nm) to 48 h (435.7 nm) resulted in the self-assembly of NPs and the formation of large NPs (Figure 4E–G). Husain et al synthesized AgNPs using an aqueous extract of *N. muscorum NCCU-442*.[48] Algal powder (1 mg) was dissolved in 2 mL of distilled water, boiled at 60 °C for 20 min and filtered using filter paper. Then, 2 mL of algal filtrate was mixed with 1 mL of 1 mM $AgNO_3$ at pH 5.5 and incubated for 24 h. The authors also controlled three optimization parameters including temperature (30, 40, 50, 60 °C), pH (3.5, 5.5, 7.5 and 9.5), and

incubation time (1, 12, 24, 48, and 72 h). These scholars found that optimum conditions for synthesizing AgNPs were a temperature of 60 °C, pH 5.5, and time period of 72 h.

Characterization of Nos@AgNPs

FTIR

FTIR spectra of the Nos@AgNPs are shown in Figure, indicating the presence of 10 infrared (IR) peaks at wavenumbers of 3419.4, 2935.4, 2850.7, 1650.9, 1535.4, 1461.4, 1338.4, 1229.4, 1082.2, and 587.7 cm^{-1} (Figure 5). These peaks correspond to the following chemical bonds: strong O-H bonds of alcohol, strong O-H bond stretching of carboxylic acid, strong N-H bond stretching of amine salts, strong C=O bond stretching of δ-lactam, strong N-O bond stretching of nitrocompound, medium C-H bending of alkane, strong C-N stretching of aromatic amine or strong S=O stretching of sulfonamide, strong C-O stretching of alkyl aryl ether, strong C-O stretching of primary alcohol, and strong C-Cl stretching of halocompounds. These data indicated that polysaccharides and proteins may be the main biomolecules that reduce AgNO$_3$ to Nos@AgNPs, whereas polysaccharides, proteins, or fatty acids stabilize Nos@AgNPs. Unfortunately, the exact reduction mechanism of NPs using algal biomass is still unclear. Theoretically, algal biomolecules such as carbohydrates, vitamins, nutrients, oil, fatty acids, polyphenols and tocopherols, carotene and xanthophyll, chlorophylls, phycobilins, nitrogenase, and NADPH-dependent reductase are the main reducing and stabilizing agent for NPs.[49,50] Husain et al analyzed the functional groups surrounding AgNPs synthesized by *N. muscorum NCCU-442* and found that the C-H bond of alkanes was absent, while the C=O and C-N bonds of amides and amines, the O-H of alcohol, and the NHC=O of the cyclic peptide cage were present at a low intensity compared to the algal extract. These results suggest that secondary metabolites are the main molecules responsible for the synthesis of AgNPs.[48] Barabadi et al synthesized AgNPs by *Penicillium fimorum* and found that phenolics and proteins were the main reductants for synthesis NPs.[51]

TEM, SEM, EDx and Mapping Analysis

TEM micrographs revealed that Nos@AgNPs had polyform shapes with dominant cubic to oval morphologies; however, some quasi-spherical and triangular NPs were detected. Nos@AgNPs were well-distributed without any agglomeration and were surrounded by thick biolayers, which could be polysaccharides, proteins, and fatty acids derived from algae during NP synthesis. The frequency distribution analysis based on 100 NP measurements showed that nanosizes ranged from 4 to 26 nm and that the average size of Nos@AgNPs was 11.8 ± 0.5 nm (Figure 6A–E). SEM micrographs showed that Nos@AgNPs were small, with cubic to spherical shapes. EDx and mapping analyses revealed that the main dominant element in Nos@AgNP samples was silver with mass% of 86.15 ± 0.23 followed
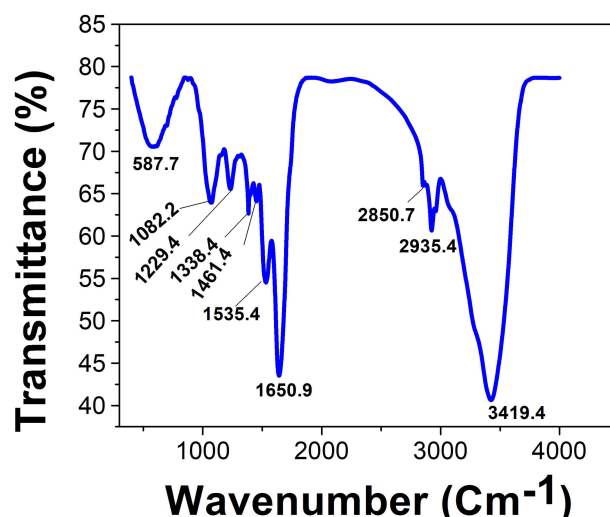

Figure 5 Functional groups surrounding Nos@AgNPs synthesized by *Nostoc muscorum* Lukesova 2/91.
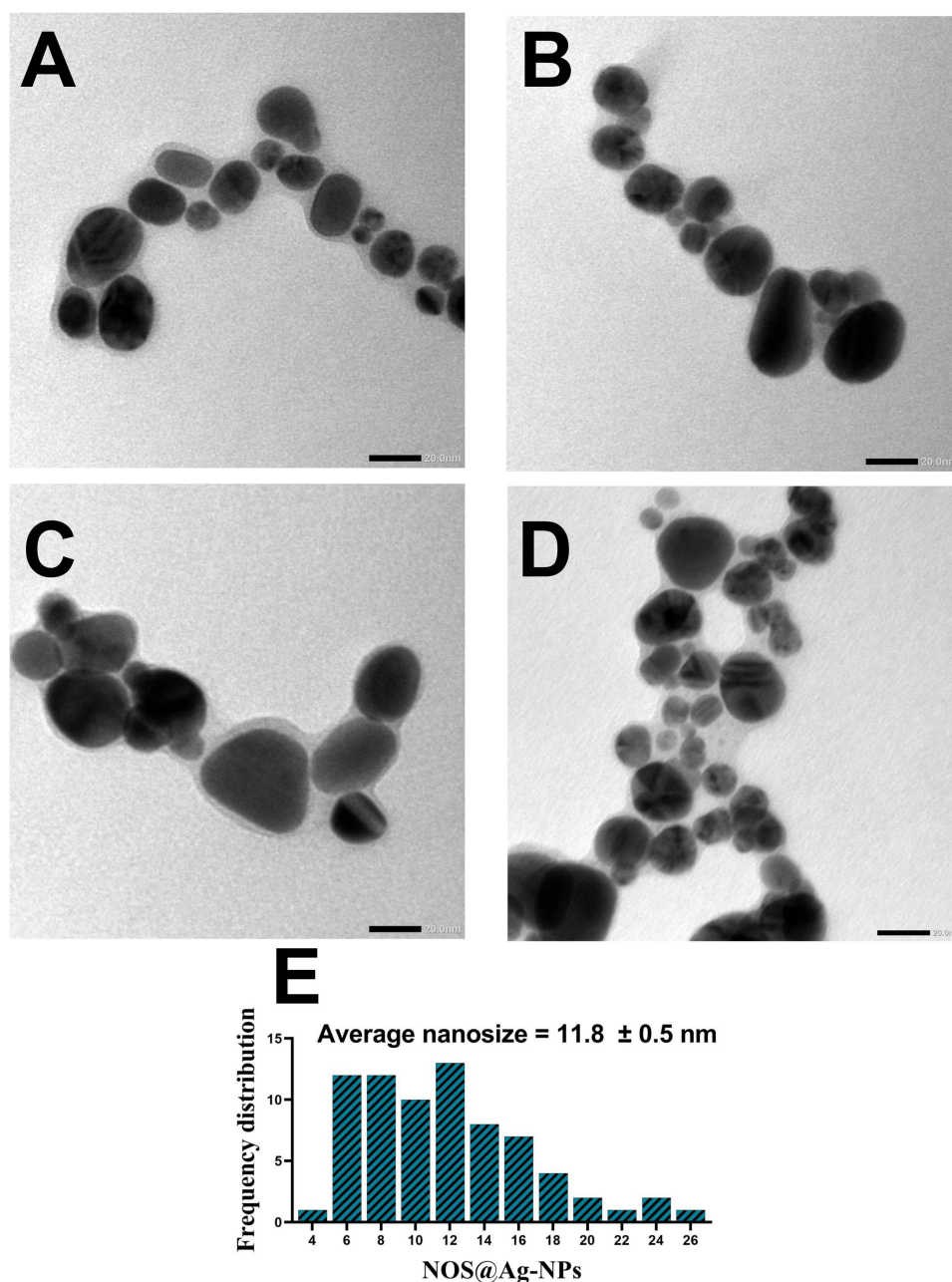
Figure 6 TEM micrographs illustrating the shape and size (**A-D**) of Nos@AgNPs synthesized by *Nostoc muscorum* Lukesova 2/91 and their average nanosize (**E**). Scale bar of 20 nm.

by carbon with mass% of 7.06 ± 0.03. These data suggest the complete synthesis of Nos@AgNPs using the algal extract (Figure 7A–D, Table 2). Other elements, such as oxygen, chloride, silica, zirconium, zinc, sulfur, and phosphorus, were present in trace amounts. These elements are essential nutrients for algal growth and are the main components of the culture medium. AgNPs synthesized using *N. muscorum NCCU-442* had a ruby-red color and a spherical shape with a nanosize of 6–45 nm and an average diameter of 30 nm.[48] After comparing the potential of *N. muscorum* Lukesova 2/91 and *N. muscorum NCCU-442* to synthesize AgNPs, we concluded that differences in strains of the same species resulted in significantly different NP physicochemical characteristics (shape, size, etc.), suggesting that the mechanisms involved in NP synthesis could be different.
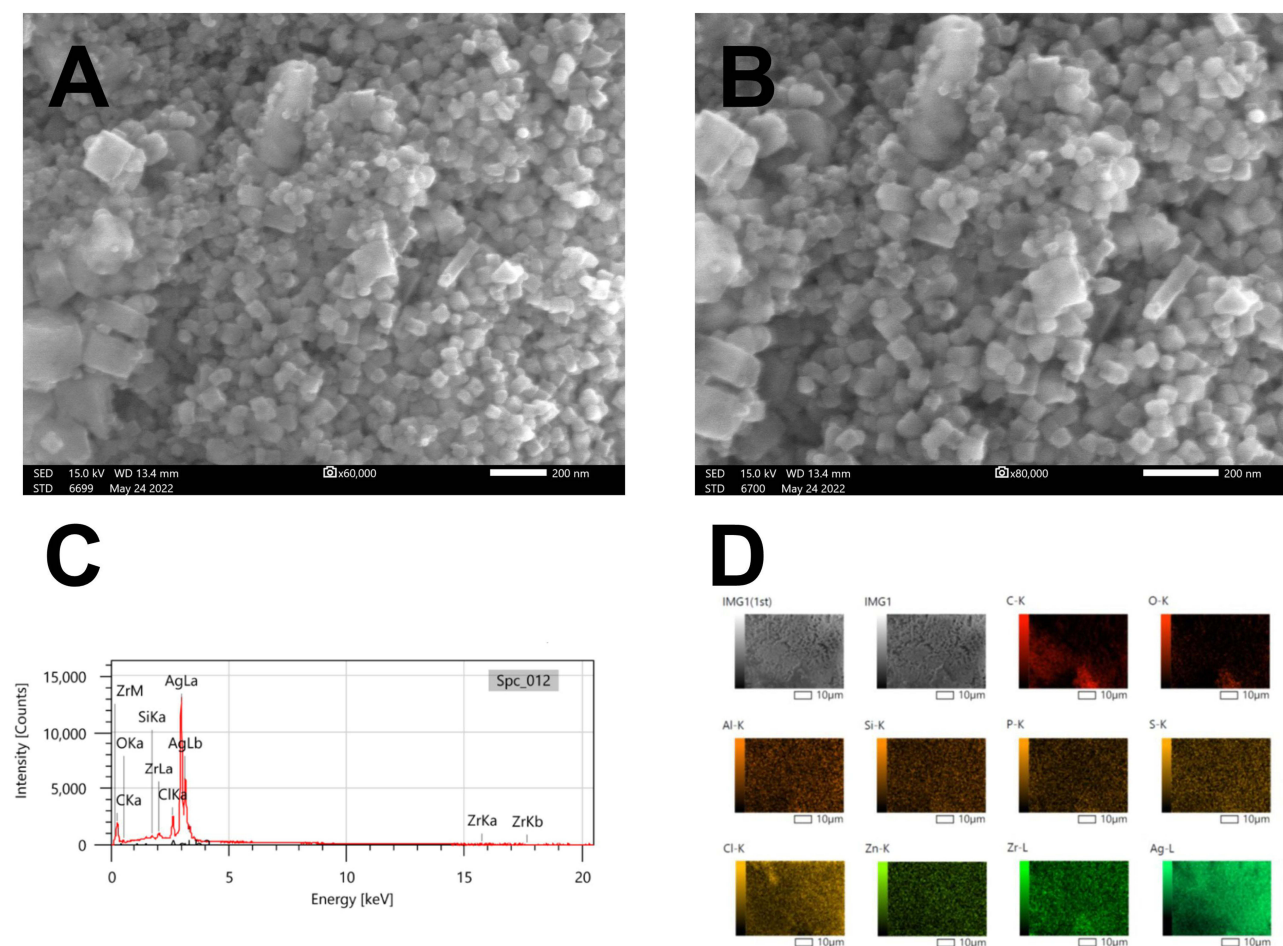
Figure 7 SEM micrographs illustrating the shape of Nos@AgNPs (**A** and **B**) synthesized by *Nostoc muscorum* Lukesova 2/91 and their EDx and mapping analyses (**C** and **D**). Of note, the mentioned map (Figure 7D) is a raw data exported from Edx software and IMG1 (1st) and IMG1 are images for the same spot as a result of routine scanning by Edx detector to enhance the electron signal. Scale bar of 200 nm.
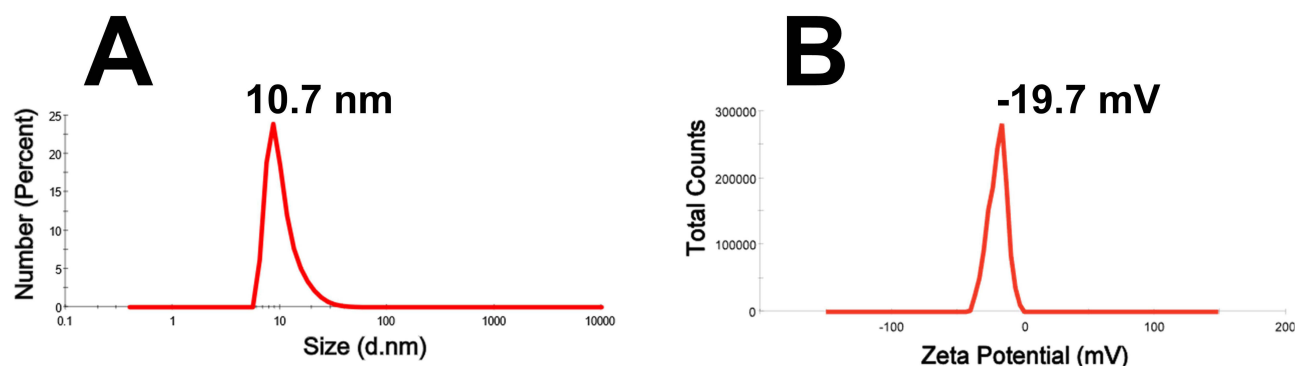
Zeta Potential and DLS

Nos@AgNPs had HDs of 10.7 nm and a potential charge of −19.7 mV (Figure 8A and B). The data of HDs of Nos@AgNPs are similar to NPs diameter calculated from TEM micrographs suggesting their stability and well

Table 2 Elemental Composition of Nos@AgNPs Synthesized by *Nostoc Muscorum* Lukesova 2/91

Element	Line	Mass%	Atom%
C	K	7.06 ± 0.03	36.87 ± 0.16
O	K	1.38 ± 0.04	5.41 ± 0.16
Si	K	0.30 ± 0.02	0.68 ± 0.05
Cl	K	3.18 ± 0.04	5.62 ± 0.06
Zr	L	1.93 ± 0.06	1.33 ± 0.04
Ag	L	86.15 ± 0.23	50.09 ± 0.13
Total		100.00	100.00

Figure 8 Hydrodynamic diameter (nm, (**A**)) and zeta potential (mV, (**B**)) of Nos@AgNPs synthesized by *Nostoc muscorum* Lukesova 2/91.
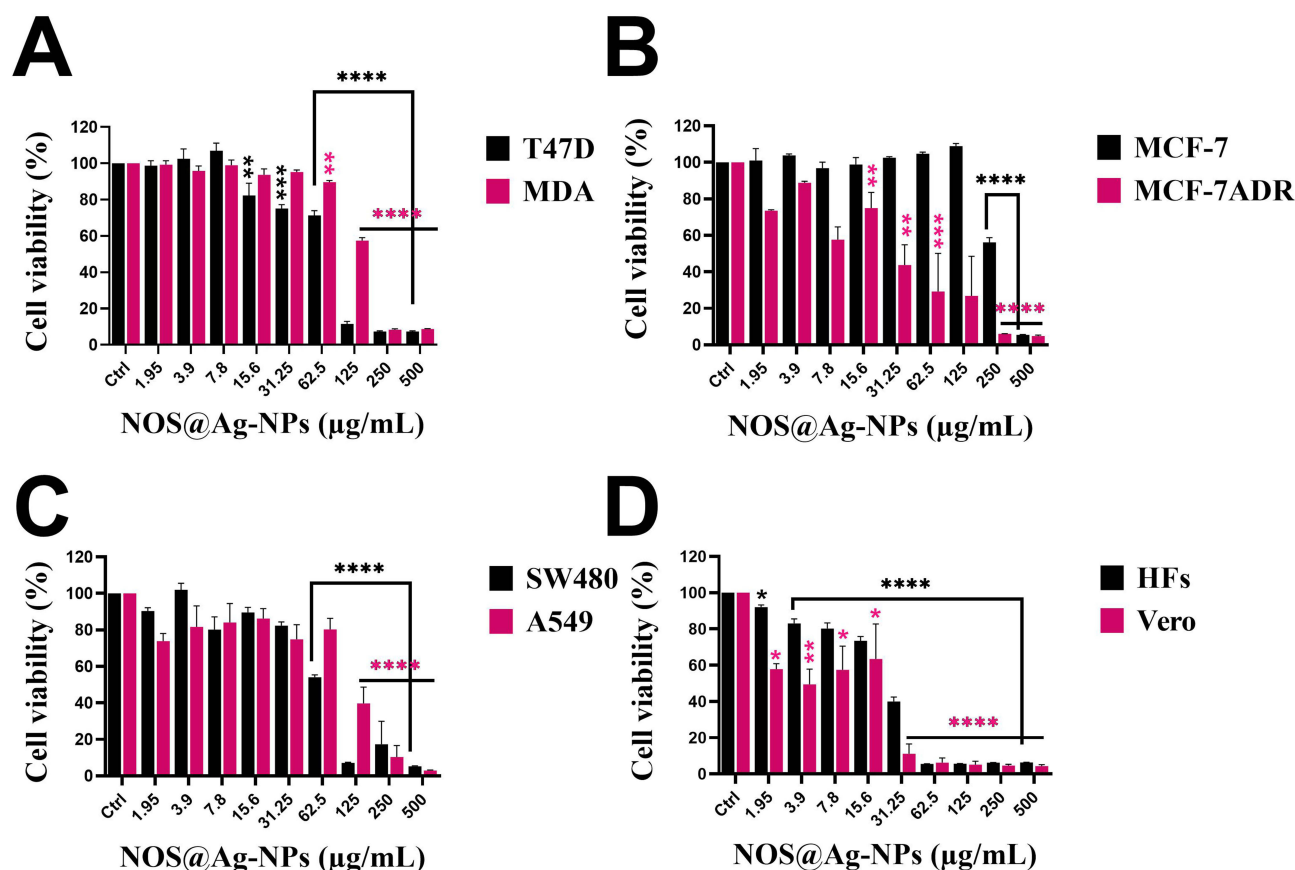
Figure 9 Inhibitory activity of Nos@AgNPs synthesized by *Nostoc muscorum* Lukesova 2/91 toward T47D, MDA-MB231 (**A**), MCF-7, MCF-7ADR (**B**), Sw480, A549 (**C**), HFs, and Vero cells (**D**). Data are presented as the mean ± SEM; *P* values were calculated versus control cells: ****$P < 0.0001$, ***$P < 0.0001$, **$P < 0.005$ and *$P < 0.01$.

dispersibility in aqueous system. The negativity of the Nos@AgNPs could be attributed to functional groups originating from the algal extracts, such as C-O and O-H. AgNPs synthesized using *N. muscorum NCCU-442* had an HD of 60 nm.[48]

Anticancer Activity

The anti-proliferative activities of Nos@AgNPs, Ch@AgNPs, 5-FU, and Doxo against breast, colon, and lung cancer cell lines were screened (Figures 9 and S1), and their IC$_{50}$ values are listed in Table 3. The data demonstrated that Nos@AgNPs significantly inhibited the viability of all tested cell types. However, lung cancer (A549) cells were the most sensitive to Nos@AgNPs, followed by T47D, MCF-7ADR, Sw480, MDA-MB231, and MCF-7 cells. The strong

Table 3 IC$_{50}$ (µg/mL) of Nos@AgNPs, Ch@AgNPs, 5-FU, and Doxo Against T47D, MDA-MB231, MCF-7, MCF-7ADR, Sw480, A549, HFs, and Vero Cells

Cells	Nos@AgNPs	Ch@AgNPs	5-FU	Doxorubicin
T47D	50.02	657	12.7	< 1000
MDA-MB231	118.1	256.9	442.7	125
MCF-7	271.9	31.18	56.48	2.394
MCF-7ADR	50.41	32.919	< 1000	1000
Sw480	81.42	28.28	49.18	1000
A549	21.56	573.4	29.85	6.447
HFs	18.78	54.06	32.43	415
Vero	5.758	18.51	33.12	< 1000

inhibitory activity of Nos@AgNPs against tumor cells can be attributed to their physicochemical characteristics, including small size to large surface area ratio, high reactivity of Ag ions to interact with cell membranes and components, negativity of their surface, and the existence of an algal corona surrounding the surface of NPs.[52,53] However, the greater cytotoxic potential of Nos@AgNPs toward lung cancer cells compared to breast and colon cancer cells could be due to the nature of the malignant cells and the mechanism of action against NPs.[35] In addition, these data indicated the selectivity of Nos@AgNPs, which may correlate with the existence of the algal corona. The crude extract of *N. commune* was found to exert significant cytotoxicity against A549 and SMMC-7721 cells; however, lung cancer cells were more sensitive than hepatic cancer cells, with an IC$_{50}$ of 24.79 and 51.33 µg/mL, respectively.[54] Among breast cancer cells, MCF-7ADR and T47D cells were the most sensitive to Nos@AgNPs, suggesting that Nos@AgNPs are potent against resistant cells. In contrast, cells most sensitive to Ch@AgNPs were Sw480 followed by MCF-7ADR, MCF-7, MDA-MB231, T47D, and A549 cells. AgNPs synthesized by *Anabaena doliolum*[55] and *N. Bahar M*[56,57] were found to have strong inhibitory activity against colon cancer colo205 cells (IC$_{50}$ of 10 µg/mL), Caco-2 cells (IC$_{50}$ of 150 µg/mL), MCF-7 cells (IC$_{50}$ of 54 µg/mL), HCT-116 cells (IC$_{50}$ of 56 µg/mL), and HepG2 cells (IC$_{50}$ of 80 µg/mL). AgNPs were synthesized extracellularly using the unicellular *ulvophyte sp*. MBIC10591, and the *Coelastrella aeroterrestrica* strain BA_Chlo4 showed potent anticancer activities against PC3 (IC$_{50}$ of 27.4 µg/mL), MDA-MB-231 (IC$_{50}$ of 20.3 µg/mL), T47D (IC$_{50}$ of 23.8 µg/mL), MCF-7 (IC$_{50}$ of 40 µg/mL), and HFs (IC$_{50}$ of 13.3 µg/mL). Additionally, the AgNPs showed potent anticancer activities against MCF-7 (IC$_{50}$ of 26.03 µg/mL) and MDA-MB231 (IC$_{50}$ of 15.92 µg/mL), HCT-116 (IC$_{50}$ of 10.08 µg/mL), and HepG2 (IC$_{50}$ of 5.29 µg/mL) cells, as well as HFs (IC$_{50}$ of 10.97 µg/mL) and Vero (IC$_{50}$ of 17.12 µg/mL) cells.[11,35] After analyzing these data, we conclude that the degree of cytotoxicity will vary according to the size of NPs, surface chemistry, and nature of tumor cells. Umapathi et al studied the anti-cancer potential of AgNPs synthesized using curcumin extract and functionalized with isonicotinic acid hydrazide in LK-2 lung cancer cells.[58] A previous study reported that AgNPs significantly inhibit the proliferative activity of malignant cells, owing to their potential to enhance reactive oxygen species formation. In contrast, NPs displayed antioxidant potential in normal lung fibroblasts (WI-38). Researchers have suggested that controlling the surface chemistry of NPs using specific biomolecules could enhance their anticancer selectivity.

Antibacterial Activity

IZ, MIC, and MBC data are shown in the Figure 10 and Table 4. The data revealed that Nos@AgNPs exhibited greater antibacterial activity against Gram-positive and Gram-negative bacteria than Ch@AgNPs and silver nitrate. However, the biocidal activity of Nos@AgNPs was greater toward *S. aureus* than other Gram-negative bacteria. Although Gram-positive bacteria have thicker cell walls than Gram-negative bacteria, Nos@AgNPs cause greater toxicity against *S. aureus* compared to other Gram-negative bacteria. This could be attributed to the charge negativity of the
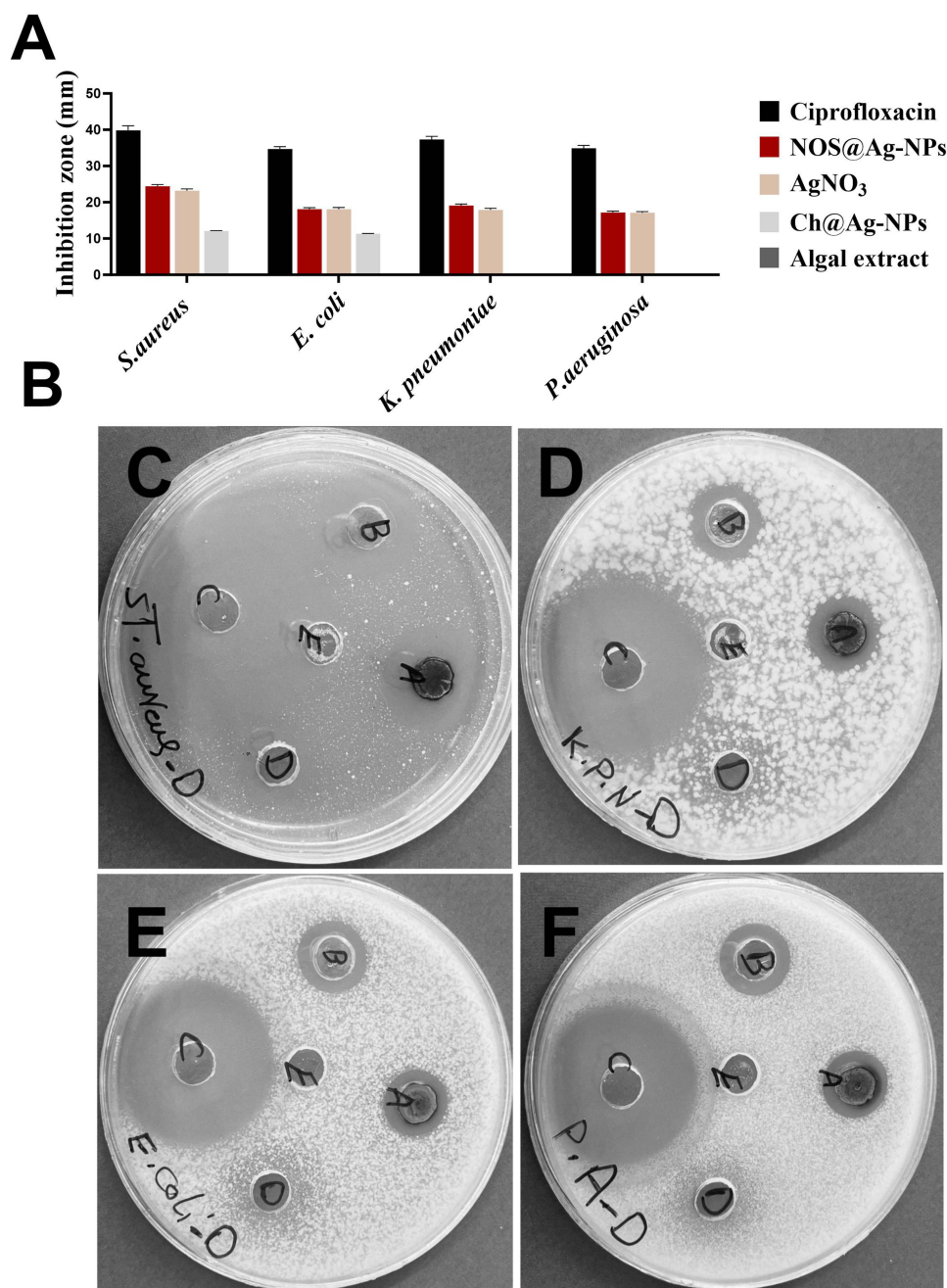
Figure 10 Antibacterial activity of Nos@AgNPs synthesized by *Nostoc muscorum* Lukesova 2/91 (represented by bar chart (**A**) and bacterial plates images (**B**)) against *S. aureus* (**C**), *K. pneumoniae* (**D**), *P. aeruginosa* (**E**), and *E. coli* (**F**). Written letters (by hand) on plates refer to (**A**) Nos@AgNPs, (**B**) AgNO₃, (**C**) ciprofloxacin, (**D**) Ch@AgNPs, and (**E**) algal extract.

Nos@AgNP surface, which enhances the electrostatic attraction between NPs and cell walls, allowing more Ag$^+$ to enter cells.[59] Our results concur with those of Husain et al, who employed AgNPs synthesized by other *N. muscorum* strain as biocidal agents against *Acinetobacter junii, E. coli* ATCC 25922, *E. coli* MTCC 443, *E. coli, K. pneumonia* ATCC 700603, *K. oxytoca, P. aeruginosa* ATCC 9027, *P. aeruginosa* MTCC 2453, and *S. aureus* MTCC 902.[48] These authors found that AgNPs significantly inhibited bacterial growth and that the highest IZ (16.0 ± 0.904 mm) was observed against *S. aureus*. However, *N. muscorum* extract and silver nitrate showed no biocidal activity against the bacteria tested. The scholars suggested that the main killing mechanism of AgNPs against bacterial cells returns to the potential of these NPs to enhance the formation of ROS.

Table 4 Inhibition Zone (IZ, Mm) of Nos@AgNPs Synthesized by *Nostoc Muscorum* Lukesova 2/91, AgNO₃, Ch@AgNPs, Algal Extract, and Ciprofloxacin Against *S. Aureus, K. Pneumoniae, P. Aeruginosa*, and *E. Coli*

Bacteria	IZ (mm)					Nos@AgNPs	
	Nos@AgNPs	AgNO₃	Ch@AgNPs	Algal extract	Ciprofloxacin	MIC	MBC
S. aureus	24.4 ± 0.23	23.2 ± 0.10	12.1 ± 0.02	0.0 ± 0.0	39.8 ± 0.42	3.9	7.8
K. pneumoniae	19.1 ± 0.14	17.9 ± 0.04	0.0 ± 0.0	0.0 ± 0.0	37.3 ± 0.23	31.25	62.5
P. aeruginosa	17.2 ± 0.03	17.1 ± 0.04	10 ± 0.001	0.0 ± 0.0	34.9 ± 0.15	31.25	62.5
E. coli	18.1 ± 0.18	18.1 ± 0.10	11.3 ± 0.01	0.0 ± 0.0	34.7 ± 0.15	15.625	62.5

Abbreviations: MTT, 3-(4,5-Dimethylthiazol-2-yl)-2,5-Diphenyltetrazolium Bromide; DMSO, Dimethyl sulfoxide; DLS, dynamic light scattering, NPs, nanoparticles; EDx, Energy Dispersive X-Ray Analysis.

Among Gram-negative bacteria, *K. pneumoniae* was the most sensitive isolate to Nos@AgNPs, suggesting that bacterial type, structure, and mechanisms could mitigate NP toxicity. Nos@AgNPs exhibited greater biocidal activity against all tested bacteria than Ch@AgNPs, suggesting that the small size and large surface area of Nos@AgNPs and the algal corona surrounding their surface may enhance their therapeutic activity. This could be attributed to i) the large surface area of NPs enabling NPs to contact the large surface area of bacteria; ii) the small size of NPs facilitating internalization of more Ag^+ into bacterial cells; and iii) the existence of an algal corona facilitating interactions between NPs and bacterial cells by targeting binding sites on bacterial membranes.[11,35] Intriguingly, *P. aeruginosa* and *E. coli* displayed the same response (same IZ values; Table) toward Nos@AgNPs and AgNO₃ suggesting that the main contributor to inhibitory activity was Ag ions in its bulk or nano-forms and/or that bacterial defense mechanisms against both Nos@AgNPs and AgNO₃ were similar. However, 1 mg/mL of *N. muscorum* Lukesova 2/91 aqueous extract was not sufficient to exert biocidal activity against the tested bacteria.[48]

Conclusion

N. muscorum Lukesova 2/91 is a cyanobacterium belonging to the *Nostoc* sp. that has moderate toxicity toward malignant cells. In this study, the potential of *N. muscorum* Lukesova 2/91 to convert AgNO₃ to AgNPs was assessed. The data revealed that *N. muscorum* Lukesova 2/91 has the potential to synthesize small NPs with excellent stability. Under optimum conditions of 1 mM of AgNO₃, 1:1 (V/V ratio of algal extract to AgNO₃), 25 °C, under light illumination for 24 h, at pH 7.4, *N. muscorum* Lukesova 2/91 synthesized Nos@AgNPs with an average diameter of 11.8 ± 0.5 nm and with cubic to oval morphologies. Nos@AgNPs were surrounded by O-H, N-H, C=O, N-O, C-H, C-N, S=O, and C-O moieties, suggesting successful synthesis of NPs using the algal isolate and indicating that proteins/polysaccharides could be the main reductants, while fatty acids (as revealed by GC-MS) could be stabilizers. Nos@AgNPs have HDs of 10.7 nm and a potential charge of −19.7 mV. Nos@AgNPs exhibited potent anticancer activity against lung, colon, and breast cancer cell lines. However, the most sensitive malignant cells were those of lung cancer cell lines. Although Nos@AgNPs exhibit greater anti-proliferative activity than other commercial anticancer drugs, they are also significantly cytotoxic to normal cells. Normal kidney cells were more sensitive to Nos@AgNPs than human fibroblasts. Nos@AgNPs displayed significant biocidal activity against *S. aureus, E. coli, K. pneumonia*, and *P. aeruginosa*; however, the greatest activity was against Gram-positive bacteria. These data suggest that *N. muscorum* Lukesova 2/91 represents an important natural resource for the biosynthesis of small NPs with potent biological activity.

Acknowledgments

Funding

Disclosure

The authors report no conflicts of interest in this work.

References

1. Arjun PNJ, Sankar B, Shankar KV, et al. Silver and Silver Nanoparticles for the Potential Treatment of COVID-19: a Review. *Coatings*. 2022;12 (11):1679. doi:10.3390/coatings12111679
2. Miu BA, Dinischiotu A. New Green Approaches in Nanoparticles Synthesis: an Overview. *Molecules*. 2022;27(19):6472. doi:10.3390/molecules27196472
3. Khan F, Shahid A, Zhu H, et al. Prospects of algae-based green synthesis of nanoparticles for environmental applications. *Chemosphere*. 2022;293:133571. doi:10.1016/j.chemosphere.2022.133571
4. Hamida RS, Ali MA, Abdelmeguid NE, et al. Lichens—A potential source for nanoparticles fabrication: a review on nanoparticles biosynthesis and their prospective applications. *J Fungi*. 2021;7(4):291. doi:10.3390/jof7040291
5. Ying S, Guan Z, Ofoegbu PC, et al. Green synthesis of nanoparticles: current developments and limitations. *Environ Technol Innovation*. 2022;26:102336. doi:10.1016/j.eti.2022.102336
6. Chetia L, Kalita D, Ahmed GA. Synthesis of Ag nanoparticles using diatom cells for ammonia sensing. *Sensing Bio-Sensing Res*. 2017;16:55–61. doi:10.1016/j.sbsr.2017.11.004
7. Kaur K, Sidhu AK, Kaur K, Sidhu AK. Green synthesis: an eco-friendly route for the synthesis of iron oxide nanoparticles. *Front Nanotechnol*. 2021;3:655062. doi:10.3389/fnano.2021.655062
8. Abdullah SM, Kolo K, Sajadi SM. Greener pathway toward the synthesis of lichen-based ZnO@ TiO2@ SiO2 and Fe3O4@ SiO2 nanocomposites and investigation of their biological activities. *Food Sci Nutrition*. 2020;8(8):4044–4054. doi:10.1002/fsn3.1661
9. Husain S, Sardar M, Fatma T. Screening of cyanobacterial extracts for synthesis of silver nanoparticles. *World J Microbiol Biotechnol*. 2015;31 (8):1279–1283. doi:10.1007/s11274-015-1869-3
10. Hamida RS, Abdelmeguid NE, Ali MA, et al. Synthesis of silver nanoparticles using a novel cyanobacteria Desertifilum sp. extract: their antibacterial and cytotoxicity effects. *Int J Nanomedicine*. 2020;Volume 15:49–63. doi:10.2147/IJN.S238575
11. Hamida RS, Ali MA, Almohawes ZN, et al. Green Synthesis of Hexagonal Silver Nanoparticles Using a Novel Microalgae Coelastrella aeroterrestrica Strain BA_Chlo4 and Resulting Anticancer, Antibacterial, and Antioxidant Activities. *Pharmaceutics*. 2022;14(10):2002. doi:10.3390/pharmaceutics14102002
12. Ssekatawa K, Byarugaba DK, Kato CD, et al. Green strategy–based synthesis of silver nanoparticles for antibacterial applications. *Front Nanotechnol*. 2021;3:697303. doi:10.3389/fnano.2021.697303
13. Sarkar K, Banerjee SL, Kundu PP, et al. Biofunctionalized surface-modified silver nanoparticles for gene delivery. *J Materials Chem B*. 2015;3 (26):5266–5276. doi:10.1039/C5TB00614G
14. Jadhav K, Deore S, Dhamecha D, et al. Phytosynthesis of silver nanoparticles: characterization, biocompatibility studies, and anticancer activity. *ACS Biomater Sci Eng*. 2018;4(3):892–899. doi:10.1021/acsbiomaterials.7b00707
15. Shantkriti S, M P. Biosynthesis of silver nanoparticles using Dunaliella salina and its antibacterial applications. *Appl Surface Sci Adv*. 2023;13:100377. doi:10.1016/j.apsadv.2023.100377
16. Roychoudhury P, Gopal PK, Paul S, et al. Cyanobacteria assisted biosynthesis of silver nanoparticles—a potential antileukemic agent. *J Appl Phycol*. 2016;28(6):3387–3394. doi:10.1007/s10811-016-0852-1
17. Varghese Alex K, Tamil Pavai P, Rugmini R, et al. Green synthesized Ag nanoparticles for bio-sensing and photocatalytic applications. *ACS omega*. 2020;5(22):13123–13129. doi:10.1021/acsomega.0c01136
18. Ghiuță I, Cristea D. *Silver Nanoparticles for Delivery Purposes, in Nanoengineered Biomaterials for Advanced Drug Delivery*. Elsevier; 2020:347–371.
19. Nath D, Banerjee P. Green nanotechnology–a new hope for medical biology. *Environ Toxicol Pharmacol*. 2013;36(3):997–1014. doi:10.1016/j.etap.2013.09.002
20. Majeed S, Saravanan M, Danish M, et al. Bioengineering of green-synthesized TAT peptide-functionalized silver nanoparticles for apoptotic cell-death mediated therapy of breast adenocarcinoma. *Talanta*. 2023;253:124026. doi:10.1016/j.talanta.2022.124026
21. Hamida RS, Ali MA, Redhwan AMO, et al. Cyanobacteria–a promising platform in green nanotechnology: a review on nanoparticles fabrication and their prospective applications. *Int J Nanomedicine*. 2020;Volume 15:6033–6066. doi:10.2147/IJN.S256134
22. Basiratnia E, Einali A, Azizian-Shermeh O, et al. Biological synthesis of gold nanoparticles from suspensions of green microalga Dunaliella salina and their antibacterial potential. *BioNanoScience*. 2021;11(4):977–988. doi:10.1007/s12668-021-00897-4
23. Caliskan G, Mutaf T, Agba HC, et al. Green Synthesis and Characterization of Titanium Nanoparticles Using Microalga, Phaeodactylum tricornutum. *Geomicrobiol J*. 2022;39(1):83–96. doi:10.1080/01490451.2021.2008549
24. Yildirim O, Ozkaya B. Effect of nanoparticles synthesized from green extracts on dark fermentative biohydrogen production. *Biomass Bioenergy*. 2023;170:106707. doi:10.1016/j.biombioe.2023.106707
25. Asif N, Ahmad R, Fatima S, et al. Toxicological assessment of Phormidium sp. derived copper oxide nanoparticles for its biomedical and environmental applications. *Sci Rep*. 2023;13(1):6246. doi:10.1038/s41598-023-33360-3
26. Hrouzek P, Ventura S, Lukešová A, et al. Diversity of soil Nostoc strains: phylogenetic and phenotypic variability. *Arch Hydrobiol Suppl Algol Stud*. 2005;117(1):251–264.

27. Chorus I, Welker M. *Toxic Cyanobacteria in Water: A Guide to Their Public Health Consequences, Monitoring and Management*. Taylor & Francis; 2021.

28. Ahmadi MA, Nourouzi B. A new report of n fixation by two species of cyanobacteria. 2008.

29. Hrouzek P, Tomek P, Lukešová A, et al. Cytotoxicity and secondary metabolites production in terrestrial Nostoc strains, originating from different climatic/ geographic regions and habitats: is their cytotoxicity environmentally dependent? *Environ Toxicol*. 2011;26(4):345–358. doi:10.1002/tox.20561

30. Princy K, Gopinath A. Optimization of physicochemical parameters in the biofabrication of gold nanoparticles using marine macroalgae Padina tetra-stromatica and its catalytic efficacy in the degradation of organic dyes. *J Nanostructure Chem*. 2018;8(3):333–342. doi:10.1007/s40097-018-0277-2

31. Hamida RS, Ali MA, Mugren N, et al. Planophila laetevirens -Mediated Synthesis of Silver Nanoparticles: optimization, Characterization, and Anticancer and Antibacterial Potentials. *ACS omega*. 2023;8(32):29169–29188. doi:10.1021/acsomega.3c02368

32. Havel J, Link H, Hofinger M, et al. Comparison of genetic algorithms for experimental multi-objective optimization on the example of medium design for cyanobacteria. *Biotechnol J*. 2006;1(5):549–555. doi:10.1002/biot.200500052

33. Bolch CJ, Orr PT, Jones GJ, et al. Genetic, morphological, and toxicological variation among globally distributed strains of Nodularia (Cyanobacteria). *J Phycol*. 1999;35(2):339–355. doi:10.1046/j.1529-8817.1999.3520339.x

34. Weisburg WG, Barns SM, Pelletier DA, et al. 16S ribosomal DNA amplification for phylogenetic study. *J Bacteriol*. 1991;173(2):697–703. doi:10.1128/jb.173.2.697-703.1991

35. Hamida RS, Ali MA, Alkhateeb MA, et al. Algal-Derived Synthesis of Silver Nanoparticles Using the Unicellular ulvophyte sp. MBIC10591: optimisation, Characterisation, and Biological Activities. *Molecules*. 2022;28(1):279. doi:10.3390/molecules28010279

36. Hamida RS, Ali MA, Alfassam HE, et al. One-Step Phytofabrication Method of Silver and Gold Nanoparticles Using Haloxylon Salicornicum for Anticancer, Antimicrobial, and Antioxidant Activities. *Pharmaceutics*. 2023;15(2):529. doi:10.3390/pharmaceutics15020529

37. Thakur RS, Ahirwar B. A steroidal derivative from Trigonella foenum graecum L. that induces apoptosis in vitro and in vivo. *j Food Drug Analysis*. 2019;27(1):231–239. doi:10.1016/j.jfda.2018.05.001

38. Lashkari A, Najafi F, Kavoosi G, et al. Evaluating the In vitro anti-cancer potential of estragole from the essential oil of Agastache foeniculum [Pursh.] Kuntze. *Biocatalysis Agr Biotechnol*. 2020;27:101727. doi:10.1016/j.bcab.2020.101727

39. Yang X, Zhang X, Yang S-P, et al. Evaluation of the antibacterial activity of patchouli oil. *Iranian j Pharm Res*. 2013;12(3):307.

40. Mazumder K, Nabila A, Aktar A, et al. Bioactive variability and in vitro and in vivo antioxidant activity of unprocessed and processed flour of nine cultivars of Australian lupin species: a comprehensive substantiation. *Antioxidants*. 2020;9(4):282. doi:10.3390/antiox9040282

41. Gushiken LFS, Beserra FP, Hussni MF, et al. Beta-caryophyllene as an antioxidant, anti-inflammatory and re-epithelialization activities in a rat skin wound excision model. *Oxid Med Cell Longev*. 2022;2022:1–21. doi:10.1155/2022/9004014

42. El-Fayoumy EA, Shanab SM, Hassan OM, et al. Enhancement of active ingredients and biological activities of Nostoc linckia biomass cultivated under modified BG-11 0 medium composition. *Biomass Conversion Biorefinery*. 2021;1–18.

43. Htwe Y, Chow WS, Suda Y, et al., Effect of silver nitrate concentration on the production of silver nanoparticles by green method. *Materials Today*, 2019;17:568–573.

44. Fu L-M, Hsu J-H, Shih M-K, et al. Process optimization of silver nanoparticle synthesis and its application in mercury detection. *Micromachines*. 2021;12(9):1123. doi:10.3390/mi12091123

45. Sibiya P, Moloto MJ. Effect of precursor concentration and ph on the shape and size of starch capped silver selenide (ag 2 se) nanoparticles. *Chalcogenide lett*. 2014;11(11):56.

46. Piñero S, Camero S, Blanco S. Silver nanoparticles: influence of the temperature synthesis on the particles' morphology. *J Phys Conf Ser*. 2017.

47. Traiwatcharanon P, Timsorn K, Wongchoosuk C. Flexible room-temperature resistive humidity sensor based on silver nanoparticles. *Mater Res Express*. 2017;4(8):085038. doi:10.1088/2053-1591/aa85b6

48. Husain S, Verma SK. Antibacterial efficacy of facile cyanobacterial silver nanoparticles inferred by antioxidant mechanism. *Mater Sci Eng*. 2021;122:111888. doi:10.1016/j.msec.2021.111888

49. Fawcett D, Verduin JJ, Shah M, et al. A review of current research into the biogenic synthesis of metal and metal oxide nanoparticles via marine algae and seagrasses. *J Nanosci*. 2017;2017:1–15. doi:10.1155/2017/8013850

50. Mukherjee A, Sarkar D, Sasmal S. A review of green synthesis of metal nanoparticles using algae. *Front Microbiol*. 2021;12:693899. doi:10.3389/fmicb.2021.693899

51. Barabadi H, Mobaraki K, Jounaki K, et al. Exploring the biological application of Penicillium fimorum-derived silver nanoparticles: in vitro physicochemical, antifungal, biofilm inhibitory, antioxidant, anticoagulant, and thrombolytic performance. *Heliyon*. 2023;9(6):e16853. doi:10.1016/j.heliyon.2023.e16853

52. Fröhlich E. The role of surface charge in cellular uptake and cytotoxicity of medical nanoparticles. *Int J Nanomedicine*. 2012;5577–5591. doi:10.2147/IJN.S36111

53. Shang L, Nienhaus K, Nienhaus GU. Engineered nanoparticles interacting with cells: size matters. *J Nanobiotechnology*. 2014;12(1):1–11. doi:10.1186/1477-3155-12-5

54. Li Z, Guo M. Healthy efficacy of Nostoc commune Vaucher. *Oncotarget*. 2018;9(18):14669. doi:10.18632/oncotarget.23620

55. Singh G, Babele PK, Shahi SK, et al. Green synthesis of silver nanoparticles using cell extracts of Anabaena doliolum and screening of its antibacterial and antitumor activity. *J Microbiol Biotechnol*. 2014;24(10):1354–1367. doi:10.4014/jmb.1405.05003

56. Bin-Meferij MM, Hamida RS. Biofabrication and antitumor activity of silver nanoparticles utilizing novel nostoc sp. *Bahar M Int J Nanomed*. 2019;Volume 14:9019–9029. doi:10.2147/IJN.S230457

57. Hamida RS, Albasher G, Bin-Meferij MM. Oxidative stress and apoptotic responses elicited by nostoc-synthesized silver nanoparticles against different cancer cell lines. *Cancers*. 2020;12(8):2099. doi:10.3390/cancers12082099

58. Umapathi A, Madhyastha H, Navya PN, et al. Surface chemistry driven selective anticancer potential of functional silver nanoparticles toward lung cancer cells. *Colloids Surf a Physicochem Eng Asp*. 2022;652:129809. doi:10.1016/j.colsurfa.2022.129809

59. Abbaszadegan A, Ghahramani Y, Gholami A, et al. The effect of charge at the surface of silver nanoparticles on antimicrobial activity against gram-positive and gram-negative bacteria: a preliminary study. *J Nanomater*. 2015;16(1):53.